Title: Reduced SARS-CoV-2 mRNA vaccine immunogenicity and protection in mice with diet-induced obesity and insulin resistance.

Authors: Timothy R. O'Meara, BA[1†], Etsuro Nanishi, MD, PhD[1, 2†], Marisa E. McGrath[3†], Soumik Barman, PhD[1,2], Danica Dong, BS[1], Carly Dillen, PhD[3], Manisha Menon, PhD[1], Hyuk-Soo Seo, PhD[4, 5], Sirano Dhe-Paganon, PhD[4, 5], Robert K. Ernst, PhD[6], Ofer Levy, MD, PhD[1, 2, 7§], Matthew B. Frieman, PhD[3§], David J. Dowling, PhD[1, 2§]

Affiliations:

[1]*Precision Vaccines Program*, Division of Infectious Diseases, Boston Children's Hospital, Boston, MA, USA 02115.

[2]Department of Pediatrics, Harvard Medical School, Boston, MA, USA 02115.

[3]Center for Pathogen Research, Department of Microbiology and Immunology, University of Maryland School of Medicine, Baltimore, MD, USA 21201.

[4]Department of Cancer Biology, Dana-Farber Cancer Institute, Boston, MA, USA 02115.

[5]Department of Biological Chemistry and Molecular Pharmacology, Harvard Medical School, Boston, MA, USA 02115.

[6]Department of Microbial Pathogenesis, University of Maryland School of Dentistry, Baltimore, MD, USA 21201.

[7]Broad Institute of MIT & Harvard, Cambridge, MA, USA 02142.

[†]These authors contributed equally to this manuscript.

[§] Co-senior authors.

Corresponding author: David J. Dowling, *Precision Vaccines Program*, Division of Infectious Diseases, Boston Children's Hospital; Harvard Medical School, Rm 842, Boston, MA 02115, USA. Tel: +1 617-919-6890. e-mail: david.dowling@childrens.harvard.edu

Author contributions: T.R.O. and E.N. conceived, designed, performed, and analyzed the experiments and wrote the manuscript; M.E.M. designed, performed, and analyzed SARS-CoV-2 neutralization experiments and mouse challenge study and wrote the paper; S.B. and M.M. performed splenocyte restimulation; S.B. performed flow cytometry and the analysis; D.D. performed qPCR experiments and their analysis; C.D., R.M.J., and M.B.F. performed and analyzed SARS-CoV-2 neutralization experiments and mouse challenge study; H.S. and S.D.P. produced the RBD protein; R.K.E. contributed to the design of experiments; O.L., M.B.F., and D.J.D. conceived the project, designed the experiments, assisted in interpretation of the results, and edited the manuscript.

Funding: The current study was supported, in part, by U.S. National Institutes of Health (NIH)/ National Institutes of Allergy and Infectious Diseases (NIAID) awards, including Adjuvant Discovery (HHSN272201400052C and 75N93019C00044) and Development (HHSN272201800047C) Program Contracts, a Massachusetts Consortium on Pathogen Readiness (Mass-CPR) award to O.L.; NIH grant (1R21AI137932-01A1) and Adjuvant Discovery Program contract (75N93019C00044) to D.J.D.; BARDA #ASPR-20-01495, DARPA #ASPR-20-01495, NIH R01 AI148166, and NIH HHSN272201400007C to M.B.F. The *Precision Vaccines Program* is supported, in part, by the BCH Department of Pediatrics and the

Chief Scientific Office. Work within the PVP on this project was funded in part by philanthropic support from Amy and Michael Barry, Stop & Shop, and the Boston Investment Conference.

Conflict of interest: E.N., T.R.O., O.L., and D.J.D. are named inventors on vaccine adjuvant patents assigned to Boston Children's Hospital, including one entitled "Adjuvants For Severe Acute Respiratory Syndrome-Related Coronavirus (SARS-CoV) Vaccines" (PCT/US21/34919). M.B.F. is on the scientific advisory board of Aikido Pharma and has collaborative research agreements with Novavax, AstraZeneca, Regeneron, and Irazu Bio. O.L.'s laboratory has received a sponsored research agreement from GlaxoSmithKline (GSK) and OL has served as a paid consultant to Moody's Analytics. D.J.D is on the scientific advisory board of EdJen BioTech and serves as a consultant with Merck Research Laboratories/Merck Sharp & Dohme Corp. (a subsidiary of Merck & Co., Inc.). These commercial or financial relationships are unrelated to the current study.

ABSTRACT

Background: Obesity and Type 2 Diabetes Mellitus (T2DM) are associated with an increased risk of severe outcomes from infectious diseases, including COVID-19. These conditions are also associated with distinct responses to immunization, including an impaired response to widely used SARS-CoV-2 mRNA vaccines.

Objective: To establish a connection between reduced immunization efficacy via modeling the effects of metabolic diseases on vaccine immunogenicity that is essential for the development of more effective vaccines for this distinct vulnerable population.

Methods: We utilized a murine model of diet-induced obesity and insulin resistance to model the effects of comorbid T2DM and obesity on vaccine immunogenicity and protection.

Results: Mice fed a high-fat diet (HFD) developed obesity, hyperinsulinemia, and glucose intolerance. Relative to mice fed a normal diet (ND), HFD mice vaccinated with a SARS-CoV-2 mRNA vaccine exhibited significantly lower anti-spike IgG titers, predominantly in the IgG2c subclass, associated with a lower type 1 response, along with a 3.83-fold decrease in neutralizing titers. Furthermore, enhanced vaccine-induced spike-specific $CD8^+$ T cell activation and protection from lung infection against SARS-CoV-2 challenge were seen only in ND mice but not in HFD mice.

Conclusion: We demonstrate impaired immunity following SARS-CoV-2 mRNA immunization in a murine model of comorbid T2DM and obesity, supporting the need for further research into the basis for impaired anti-SARS-CoV-2 immunity in T2DM and investigation of novel approaches to enhance vaccine immunogenicity among those with metabolic diseases.

Word count: 231

Capsule summary: Obesity and type 2 diabetes impair SARS-CoV-2 mRNA vaccine efficacy in a murine model.

Keywords: SARS-CoV-2, mRNA vaccine, immunogenicity, obesity, type 2 diabetes

Abbreviations: Type 2 diabetes mellitus, T2DM; diet-induced obesity, DIO; antibody, Ab; high-fat diet, HFD; receptor-binding domain, RBD; normal diet, ND; intraperitoneal glucose tolerance test, IPGTT; interferon, IFN; IFN-stimulated genes, ISGs; dendritic cell, DC.

INTRODUCTION

The size and proportion of the population with obesity and diabetes mellitus (DM) are growing across the globe, especially in high-income countries. Among US adults, the prevalence of obesity and DM are 41.9% and 14.8%, respectively[1]. The relationship between DM and an increased risk of morbidity and mortality caused by a variety of infectious diseases has long been recognized, especially in older adults with DM[2]. Similarly, DM and obesity are risk factors of severe COVID-19 or death, along with other factors such as older age, male sex, and underlying comorbidities (e.g., cardiovascular disease and chronic kidney disease)[3-6]. The prevalence of these metabolic disorders indicates an urgent need to prevent the incidence of severe infections, specifically COVID-19, in these vulnerable populations to reduce disease burden.

Despite improving overall disease outcomes, many currently approved vaccines, including the SARS-CoV-2 BNT162b2 mRNA vaccine, are not as effective in patients with DM or obesity. Following the introduction of mRNA vaccines against SARS-CoV-2, clinical studies found that Type 2 DM (T2DM) is associated with significant reductions in both humoral and cellular responses to vaccination against SARS-CoV-2, particularly among those with poor glycemic control[7, 8]. Reduced vaccine immunogenicity has been observed among adults, especially men, with obesity[9]. Together, these findings suggest that metabolic diseases impair vaccine responses and increase the risk of severe COVID-19. However, the exact effects of metabolic disease on the quality of humoral and cellular immune responses remain unclear. There is therefore a need to assess the causes of impaired vaccine response in those with metabolic disease and evaluate what aspects of immunity are affected to inform optimization of vaccine approaches for this vulnerable population.

While our understanding of the influence of obesity and T2DM on SARS-CoV-2 vaccine responses remains limited, murine models of diet-induced obesity (DIO) and insulin resistance have facilitated initial studies of the connections between metabolic disease, immunity, and viral disease pathology, particularly in the context of influenza. Following infection with influenza, DIO mice exhibited higher lung damage and mortality[10-14]. Further, DIO mice mounted impaired immune responses following immunization with subunit or inactivated-virus influenza vaccines, including decreased antibody (Ab) titers relative to controls, lower $CD8^+$ T cell levels, impaired protection from live viral challenge, and greater waning in humoral immunity[15-18]. Additionally, studies of MERS-CoV and SARS-CoV-2 infection have found that DIO mice exhibit increased lung titers and/or greater morbidity and mortality following live-virus challenge relative to controls[19-21]. However, little is known regarding the effects of obesity and hyperglycemia on SARS-CoV-2 vaccine responses. Furthermore, no studies have yet evaluated the effects of obesity and hyperglycemia on mRNA vaccine immunogenicity in detail despite the widespread use of mRNA-based SARS-CoV-2 vaccines in the clinic.

We therefore sought to address these gaps by evaluating the effects of obesity and T2DM on Ab levels and function, T cell responses, and protection from live SARS-CoV-2 challenge in animals that received the SARS-CoV-2 BNT162b2 mRNA vaccine. To this end, we established a mouse model of obesity, hyperinsulinemia, and glucose intolerance using a high-fat diet (HFD) and then immunized mice with BNT162b2 or an alum adjuvanted SARS-CoV-2 spike receptor-binding domain (RBD) subunit vaccine. We then assessed binding and neutralizing Ab titers, $CD8^+$ T cell activation, and protection from infection during viral challenge. We found that

HFD-induced obesity and T2DM impaired both humoral and cellular immune responses post-BNT162b2 immunization. HFD-fed mice had significantly lower neutralizing titers and IgG2c titers compared to mice fed with a normal diet (ND). Furthermore, while ND mice exhibited RBD-specific $CD8^+$ T cell activation, T cell activation profiles were not significantly enhanced in HFD mice when compared to a PBS-injected control. In line with these immunogenicity data, lung viral titers and inflammation profiles after viral challenge were only significantly reduced relative to the PBS-injected group among ND mice, while no significant reduction versus the PBS group was observed in the HFD group. Overall, our study demonstrates that diet-induced obesity and T2DM in a murine model reduce immunogenicity and protective efficacy of the SARS-CoV-2 BNT162b2 mRNA vaccine, laying the groundwork for further study of the mechanisms of these deficiencies and strategies that can be used to overcome them.

RESULTS

A high-fat diet causes weight gain, hyperinsulinemia, and glucose intolerance in male C57BL/6J mice.

We first confirmed that feeding a HFD led to diet-induced obesity (DIO), fasting hyperinsulinemia, and glucose intolerance in male C57BL/6J mice as previously observed for this model[21-23]. To this end, mice were fed a HFD containing 60% kcal from fat or a ND containing 10% kcal from fat beginning at age 6 weeks (**table S1**). Animals were transferred from the supplier at 15 weeks old, allowed to acclimate for two weeks, and weighed weekly through the post-vaccination blood draw at 30 weeks of age. After feeding mice the HFD for 18 weeks, fasting serum insulin was measured. Glucose intolerance was measured via an intraperitoneal glucose tolerance test (IPGTT) the following week (**Fig. 1A**). As expected, mice that received a HFD were significantly heavier than mice fed a ND throughout the experiment ($P < 0.0001$ at all time points, **Fig. 1B**). The HFD mice were visually distinct from the ND mice, appearing much wider and rounder throughout the experiment (**fig. S1**). During the week of the prime vaccination, HFD mice ranged from 37.2 to 61.2 g, with an average weight of 48.8 g, while ND mice ranged from 26.9 to 36.8 g, averaging 31.8 g (**Fig. 1C**). In addition to weight gain, HFD mice also developed hyperinsulinemia, with significantly elevated fasting serum insulin levels as compared to ND mice at age 24 weeks ($P < 0.0001$, **Fig. 1D**). Further, serum insulin demonstrated a significant positive correlation with weight in both the ND mice ($r = 0.4369$, $P = 0.0061$) and HFD mice ($r = 0.6194$, $P < 0.0001$), suggesting an association between weight gain and hyperinsulinemia, particularly in mice that received a HFD (**Fig. 1E**). Finally, we employed an IPGTT to assess glucose intolerance in HFD mice versus ND mice (**Fig. 1F, G**). HFD mice had a significantly higher median blood glucose following a 6-hour fast than ND mice

(244 mg/dL vs. 170 mg/dL, $P < 0.0001$, **Fig. 1G**). Following intraperitoneal injection of 2 g/kg dextrose, HFD mice maintained significantly higher blood glucose measurements than ND mice at 30, 75, and 120 minutes after injection ($P < 0.0001$ for all comparisons, **Fig. 1F**) and ended at a median of 600 mg/dL versus 225 mg/dL in ND mice (**Fig. 1G**). Moreover, 21 of the 38 HFD mice remained > 600 mg/dL, the blood glucose meter's upper limit of detection, at the final time point (120 minutes after injection), in contrast with none of the ND mice (**Fig. 1G**).

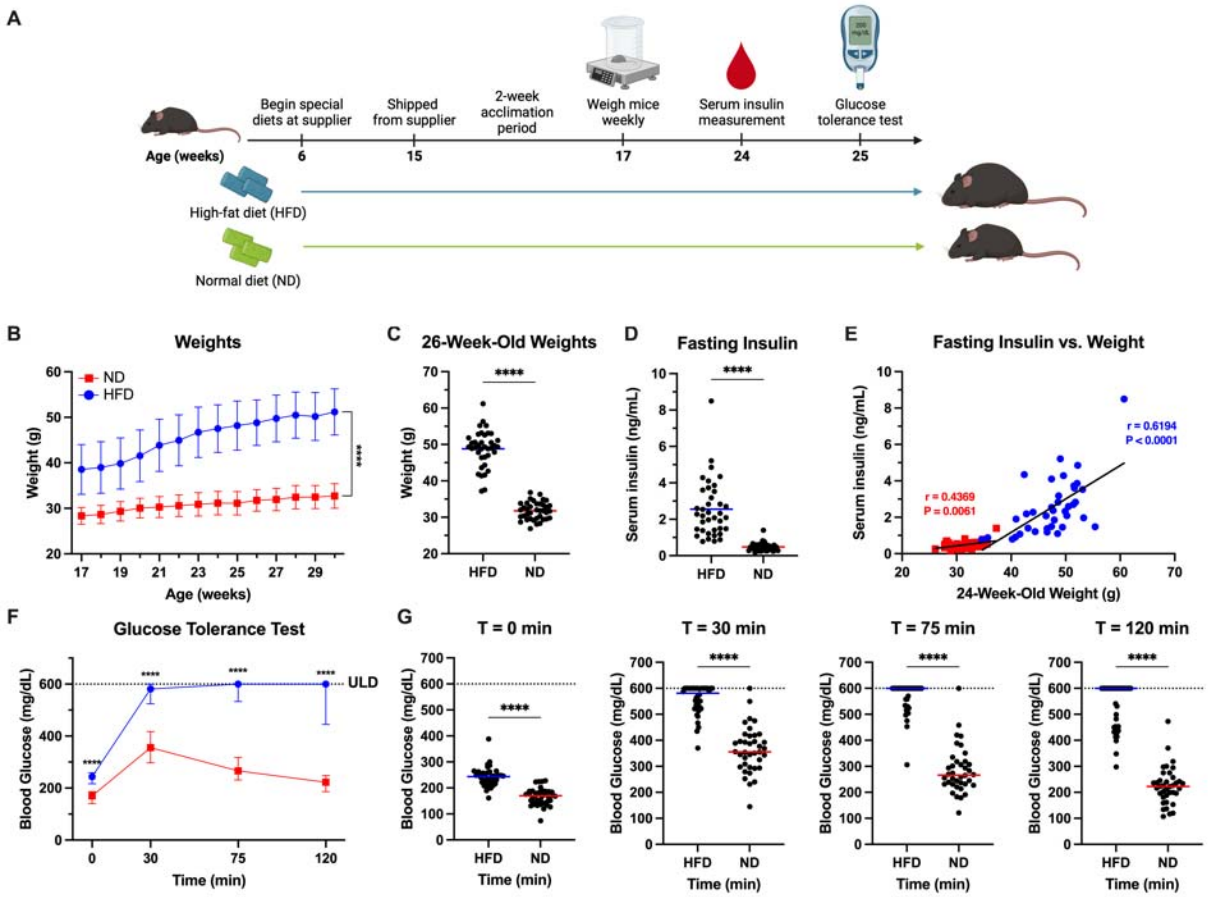

Figure 1. Male C57BL/6J mice fed a high-fat diet develop obesity, hyperinsulinemia, hyperglycemia, and poor glucose tolerance.

Male C57BL/6J mice were fed a high-fat diet (HFD) consisting of 60% kcal from fat or an ingredient-matched control diet containing 10% kcal from fat (normal diet, ND) beginning at age 6 weeks. Mice were transferred from the vendor at 15 weeks old and allowed to acclimate for two weeks following receipt. Mice were then weighed weekly to assess weight gain. At 24 weeks old, serum insulin was measured by ELISA following a 6-hour fast. The following week, an intraperitoneal glucose tolerance test was performed to assess glucose tolerance. (**A**) Experimental design. (**B**) Mouse weights during the study. (**C**) Weights at 26 weeks of age. (**D**) Serum insulin levels measured at 24 weeks of age after a 6-hour fast. (**E**) Pearson's correlation analysis was used to examine the correlation between serum fasting insulin levels and weights at 24 weeks of age. Lines indicate linear regression. (**F, G**) Glucose tolerance was assessed by measuring blood glucose at time points 0, 30, 75, and 120 min following a 6-hour fast and intraperitoneal injection of 2 g/kg dextrose. Blood glucose values above the glucometer's 600 mg/dL upper limit of detection (ULD) were assigned a value of 600 mg/dL. N = 38 per group in all experiments. Longitudinal graphs display mean and standard deviation (**B)** or median and IQR (**F**). Bars represent means (**C, D**) or medians in all dot plots (**G**). Significance was assessed by unpaired t-test (**B–D**) or Mann-Whitney U-tests (**F, G**), correcting for multiple comparisons when relevant. **** $P < 0.0001$.

HFD mice elicited impaired antibody responses following SARS-CoV-2 mRNA vaccination. Following establishment of the comorbid obesity, hyperinsulinemia, and glucose intolerance phenotypes, mice were immunized with SARS-CoV-2 BNT162b2 mRNA or a protein subunit vaccine benchmark vaccine at a 2-dose regimen with a 14-day interval to assess the effects of the HFD on vaccine immunogenicity and protective efficacy (**Fig. 2A**). Mice were randomly assigned to receive 1 µg of SARS-CoV-2 BNT162b2 mRNA (Comirnaty®), or 10 µg of recombinant monomeric SARS-CoV-2 spike RBD protein formulated with 100 µg of aluminum hydroxide (Alhydrogel®). Within the HFD or ND mice, each vaccine treatment group had generally comparable weights, insulin levels, and IPGTT results (**Fig. S2**). Immunizations were given intramuscularly to mice at 26 and 28 weeks of age. Two weeks after the 2nd immunization, humoral immunity was assessed.

In ND mice, robust humoral responses were observed after BNT162b2 immunization, while an alum-adjuvanted RBD subunit vaccine induced limited Abs (**Fig. 2B–E**). Importantly, among mice that received BNT162b2, there was a 2.2-fold reduction in anti-spike IgG in HFD mice compared to ND mice ($P = 0.0002$, **Fig. 2B**). In further IgG subclass assessment, there was a large reduction in anti-spike IgG2c in HFD mice compared to ND mice post BNT162b2 immunization (GMTs of 105191 vs. 14250, $P < 0.0001$, **Fig. 2B**) although the difference in IgG1 titers was not significant. Accordingly, the Ab response was significantly skewed toward IgG2c in ND mice relative to HFD mice, with mean IgG2c:IgG1 ratios of 2.81 versus 0.87, respectively ($P = 0.002$, **Fig. 2B**). RBD plays a key role in ACE2 binding and is the main target of neutralizing Abs. We thus assessed anti-RBD IgG titers and confirmed a significant reduction in anti-RBD IgG2c in HFD mice compared to ND mice post BNT162b2 immunization (**Fig. 2C**).

To analyze Ab function, we next performed a surrogate of virus neutralization test that measures the degree of inhibition of RBD binding to hACE2 by immune sera, as well as a neutralization assay with live SARS-CoV-2 virus. HFD mice exhibited significantly impaired hACE2-RBD binding inhibition and live virus neutralization relative to ND mice post BNT162b2 immunization ($P < 0.0001$ and $P = 0.0003$ respectively, **Fig. 2D, E**). To assess the effects of obesity and T2DM on humoral immunity individually, correlations between either weight at the time of immunization or fasting insulin, measures associated with obesity and diabetic phenotypes, respectively, and Ab responses were assessed in HFD mice. Interestingly, serum insulin, but not weight, negatively correlated with anti-spike IgG2c titers ($P = 0.016$ and $P = 0.334$ respectively, **Fig. 2F, G**). Overall, these results demonstrate that, relative to control mice fed a ND, HFD mice mount impaired Ab responses following immunization with BNT162b2, marked by a reduction in anti-spike IgG titers, a lower IgG2c:IgG1 ratio, impaired inhibition of hACE2-RBD binding, and a reduction in live virus neutralizing titers.

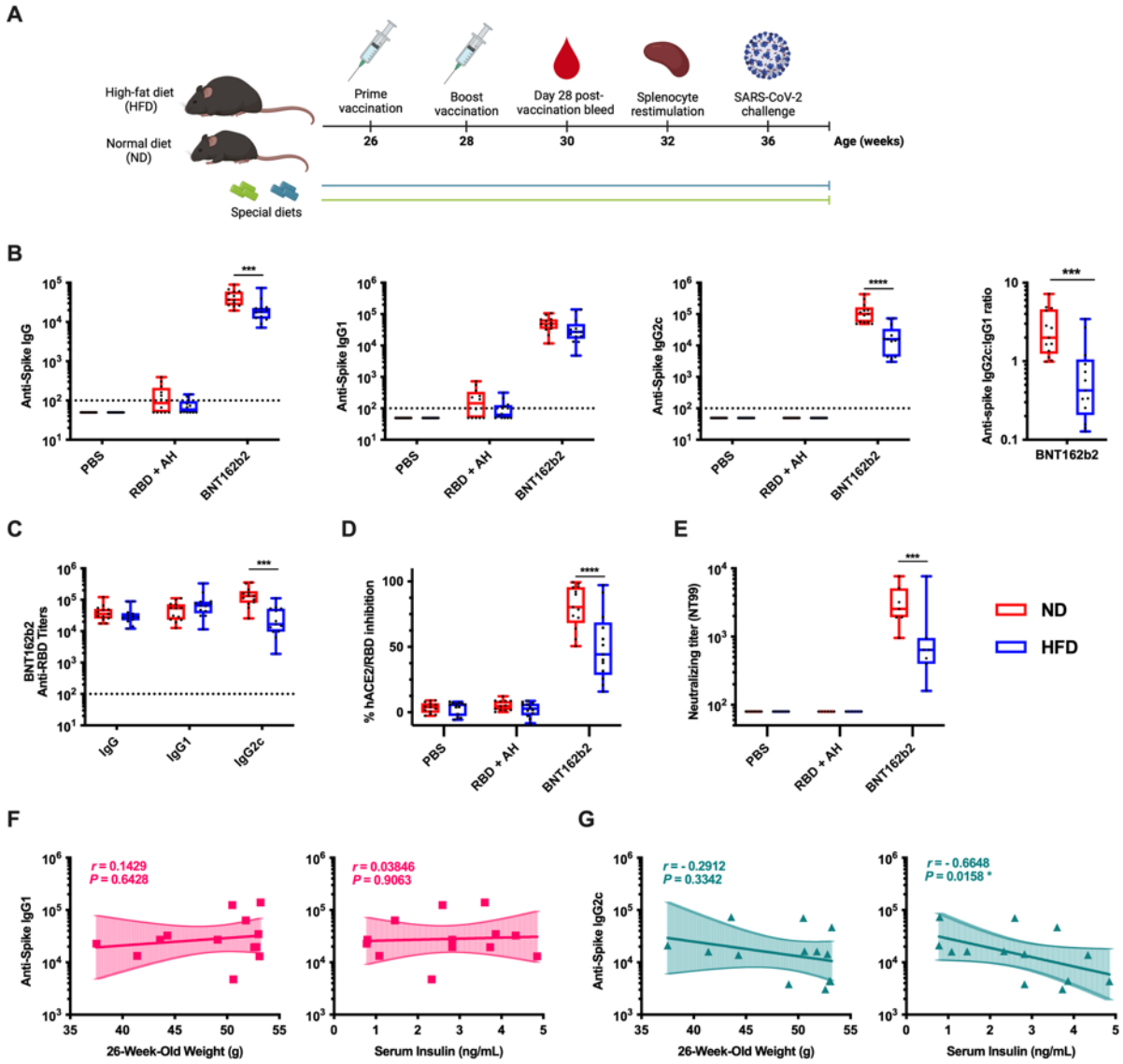

Figure 2. SARS-CoV-2 mRNA vaccine elicits reduced humoral immunogenicity in HFD mice.

Male C57BL/6J mice fed with high-fat diet (HFD) or normal diet (ND) were immunized intramuscularly with a 2-dose regimen with 10 µg of aluminum-adjuvanted recombinant RBD or 1 µg of BNT162b2 mRNA. Serum samples were collected 14 days after the final immunization. (**A**) Experimental schematic. (**B–E**) Anti-Spike IgG, IgG1, IgG2c, and IgG2c:IgG1 ratio (**B**), Anti-RBD IgG, IgG1, and IgG2c post BNT162b2 mRNA immunization (**C**), hACE2-RBD inhibition rate (**D**), and WA1 SARS-CoV-2 neutralizing titers (**E**) were assessed. Dashed lines represent lower limits of detection. After log transformation, data were analyzed by two-way ANOVA followed by post-hoc tests for multiple comparisons. * $P < 0.05$, ** $P < 0.01$, *** $P < 0.001$, and **** $P < 0.0001$. (**F-G**) Correlations between anti-spike IgG1 (**F**) or IgG2c (**G**) titers and weight at vaccination or fasted serum insulin at 24 weeks of age of HFD mice following BNT162b2 mRNA immunization were assessed with Spearman's rank correlation. Lines indicate linear regression. N = 12-13 per group except for neutralizing titers (N = 6-7 mice per group).

HFD mice exhibit impaired CD8$^+$ T cell activation following SARS-CoV-2 mRNA vaccination.

SARS-CoV-2 spike specific CD8$^+$ T cells are elicited by mRNA vaccines and contribute to protection against SARS-CoV-2 [24-26]. We therefore analyzed spike RBD-specific CD8$^+$ T cell responses of the HFD and ND mice 4 weeks after the final immunization. Splenocytes were collected and stimulated with overlapping peptides of the wildtype SARS-CoV-2 spike RBD. Intracellular expression of interferon-γ (IFNγ), TNF, and IL-2 in CD8$^+$ T cells was assessed by flow cytometry to quantify antigen-specific cytotoxic T cell responses (**Fig. 3A**). As expected, BNT162b2 immunization elicited significantly higher CD8$^+$ T cell expression of IFNγ, TNF, and IL-2 than PBS injection in ND mice (P = 0.002, P = 0.007, and P = 0.010, respectively), while alum-adjuvanted RBD subunit vaccine was not significant versus PBS for any cytokines (**Fig. 3B–D**). In contrast, neither BNT162b2 nor alum-adjuvanted RBD significantly induced CD8$^+$ T cell IFNγ, TNF, or IL-2 expression versus PBS among HFD mice (**Fig. 3B–D**). While only the ND mice exhibited a significant vaccine-induced increase in cytokine expression over their corresponding PBS group, there was not a significant difference in cytokine expression comparing HFD and ND mice when compared head-to-head within the BNT162b2 vaccination condition (**Fig. 3B–D**). However, the median percentages of IFNγ, TNF, and IL-2 positive CD8$^+$ T cells were all at least 2-fold greater in ND mice than in HFD mice (2.4-, 2.0-, and 2.9-fold, respectively). Overall, significant CD8$^+$ T cell activation was observed in ND but not HFD mice that received the SARS-CoV-2 BNT162b2 mRNA vaccine, indicating an impaired antigen-specific CD8$^+$ T cell Spike response in HFD mice.

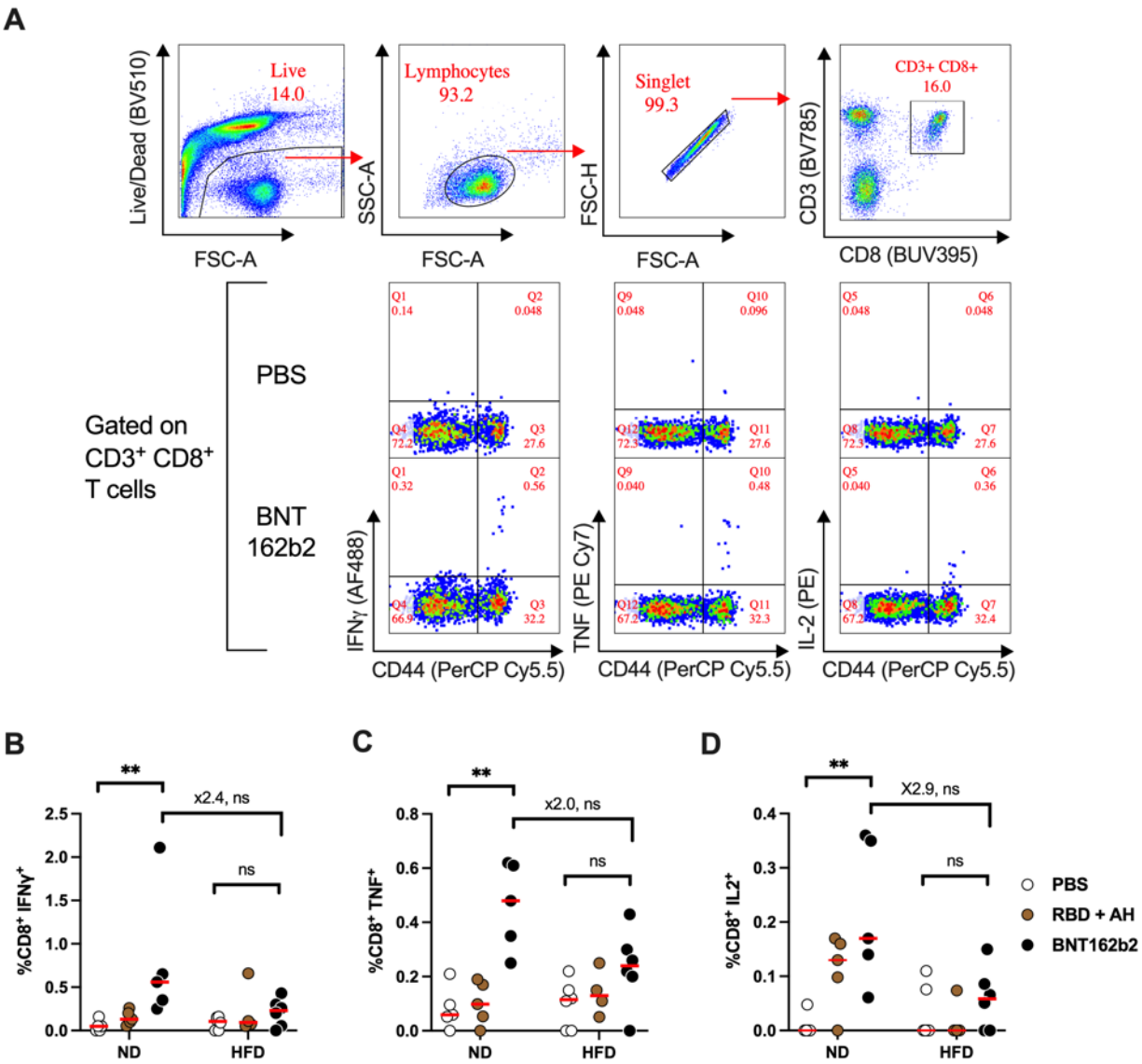

Figure 3. SARS-CoV-2 mRNA vaccine enhances CD8$^+$ T cell responses in ND but not HFD mice.

Male C57BL/6J mice fed with high-fat diet (HFD) or normal diet (ND) were immunized as in Figure 2. Splenocytes were collected 4 weeks after the final immunization and stimulated with a SARS-CoV-2 spike RBD peptide pool. (**A**) Representative flow data. (**B-D**) Expression of intracellular IFNγ (**B**), TNF (**C**), and IL-2 (**D**) was assessed by flow cytometry in CD8$^+$ T cells. **N** = 4-6 per group. Bars represent median. Dots represent individual values. Data were analyzed by the Kruskal-Wallis Test adjusted for multiple comparisons. Fold difference between BNT162b2-immunized ND and HFD mice are shown. ** $P < 0.01$.

SARS-CoV-2 mRNA vaccine protects ND mice but not HFD mice from lung infection.

To assess vaccine efficacy, we challenged immunized mice with live SARS-CoV-2. Eight weeks after the final immunization, mice were challenged intranasally with 10^3 PFU of mouse-adapted MA10 SARS-CoV-2[27] , as indicated in **Fig. 2A**. Mice were weighed before infection, and the HFD mice remained significantly heavier, with a mean weight of 52.7 g versus a mean of 34.0 g among ND mice ($P < 0.0001$). Two days after infection, mice were euthanized, and lungs were harvested for analysis. Minor inflammation was seen in all lung samples, though differences between groups were undetectable in line with the early timepoint following infection (**fig. S3**).

To determine protective efficacy, host lung inflammatory responses were evaluated by assessing gene expression of cytokines, chemokines, and IFN-stimulated genes (ISGs) associated with SARS-CoV-2 severity including *Ifit2*, *Cxcl10*, *Csf2*, *Il6*, *Ccl2* and *Cxcl1*[28-32]. PBS-injected HFD and ND mice both demonstrated high inflammatory responses across multiple genes (**Fig. 4A**). Of note, BNT162b2-immunized ND mice demonstrated significant lower gene expression relative to PBS group, while there was no significant difference between HFD mice that received PBS or BNT162b2 (**Fig. 4A**). To further determine protective efficacy, lung viral titers were analyzed (**Fig. 4B**). Naive, PBS-injected mice demonstrated robust viral loads in both HFD and ND mice (geometric means: 1.58×10^8 and 6.20×10^9, respectively). In line with the low immunogenicity data, both HFD and ND mice vaccinated with alum-adjuvanted RBD were not protected from lung infection (geometric means: 2.61×10^7 and 3.80×10^8 in HFD and ND mice respectively, **Fig. 4B**). Similar to the pattern of expression observed for inflammatory genes, ND mice that received BNT162b2 exhibited a significant decrease in lung viral titer relative to the PBS group ($P = 0.004$), while there was no significant difference between HFD mice that

received PBS or BNT162b2 (P = 0.535, **Fig. 4B**). Compared to HFD, ND mice that received BNT162b2 demonstrated a 262-fold reduction in lung viral titers (geometric means: 9.25×10^6 and 3.53×10^4 in HFD and ND mice, respectively), though this difference was not statistically significant (P = 0.175, **Fig. 4B**). Lastly, to define immune correlates of protection, we assessed correlations between neutralizing titers and challenge study readouts. Neutralizing titers demonstrated strong inverse correlations with *Ifit2* gene expressions ($r = -0.8166$, $P < 0.0001$) and lung viral loads ($r = -0.6640$, P = 0.0002) (**Fig. 4C**). Although one HFD mouse with high neutralizing titer demonstrated high lung viral titer, the mouse was protected from lung inflammation with suppressed *Ifit2* expression (arrow, **Fig 3C**). Overall, these results demonstrate that HFD mice are not protected from infection with SARS-CoV-2 following immunization with BNT162b2, while ND mice are significantly protected against viral lung infection after receiving BNT162b2.

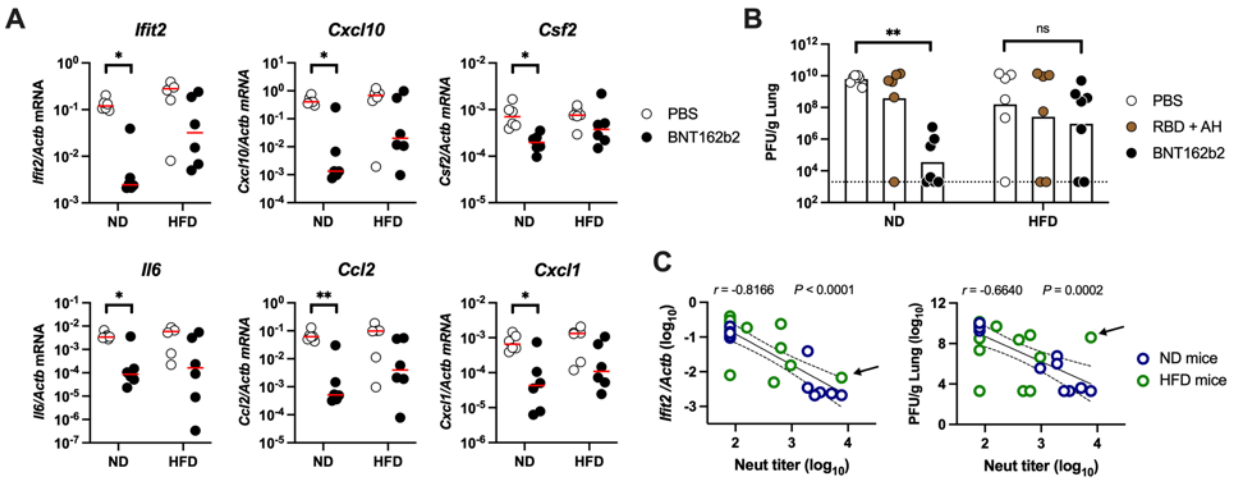

Figure 4: SARS-CoV-2 mRNA vaccine protects ND mice but not HFD mice.
Male C57BL/6J mice fed high-fat diet (HFD) or normal diet (ND) were immunized as in Figure 2. Six weeks after immunization, mice were challenged with 10^3 PFU of MA10 SARS-CoV-2. Mice were euthanized 2 days after infection and lungs were harvested for analysis. (**A, B**) To assess protective efficacy, lung homogenates were analyzed for gene expression profiles of *Ifit2*, *Cxcl10*, *Csf2*, *Il6*, *Ccl2* and *Cxcl1* shown as relative expression compared to *Actb* (**A**) and viral titers (**B**). Bars represent medians (**A**) or geometric means (**B**). Dashed lines represent lower limits of detection. n = 6–7 per group. Data were analyzed by the Mann-Whitney or Kruskal–Wallis test corrected for multiple comparisons. **P* < 0.05, ***P* < 0.01. (**C**) Correlations between neutralizing titers and gene expressions of *Ifit2* over *Actb* and lung viral loads are shown. Circles represent individual mice that received PBS or BNT162b2, and colors indicate ND or HFD mice. Solid and dashed lines respectively indicate linear regression and 95% confidence interval. Correlations were assessed by two-sided Pearson tests. Arrow represents one HFD mouse with high neutralizing titer showing high lung viral titer but suppressed *Ifit2* expression.

DISCUSSION

Overall, we have shown for the first time that HFD-induced insulin resistance and obesity impair SARS-CoV-2 mRNA vaccine humoral and cellular immunogenicity, providing causal evidence to support observations in human patients and establishing a model for studying the relationship between metabolic diseases and SARS-CoV-2 vaccine responses. T2DM and obesity are known risk factors for severe COVID-19 and have been correlated with reduced responses to mRNA vaccines against SARS-CoV-2[7-9, 33]. However, a causal link between these conditions and impaired vaccine responses has not yet been established. Using DIO mouse models, previous studies have recapitulated pathological findings of MERS-CoV and SARS-CoV-2 observed in humans, establishing this model as a viable option for studying the relationship between metabolic disease and SARS-CoV-2 vaccine response[19-21]. Here, we developed a mouse model of metabolic disease by feeding mice a HFD, which led to obesity, hyperinsulinemia, and glucose intolerance. We then immunized mice with SARS-CoV-2 mRNA BNT162b2 vaccine, an alum-adjuvanted RBD subunit vaccine, or a PBS control, after which we assessed Ab and T cell responses and protection from viral challenge. We found that HFD mice exhibited an overall reduction in BNT162b2 response relative to ND mice, marked by a reduction in neutralizing Abs. We also observed significantly enhanced RBD-specific $CD8^+$ T cell induction only in ND mice but not in HFD mice. Furthermore, BNT162b2-vaccinated HFD mice exhibited a lack of protection from live viral challenge relative to PBS-injected HFD mice, while BNT162b2-vaccinated ND mice demonstrated protection relative to the PBS-injected ND mice.

We observed that in HFD mice, BNT162b2 vaccine demonstrated a consistent and cumulative pattern of reduced immunogenicity across multiple measures, including binding and neutralizing

Ab titers and $CD8^+$ T cell activation. Interestingly, while antigen-specific IgG1 titers were comparable among HFD and ND mice, the induction of IgG2c Abs was substantially reduced in HFD mice relative to ND mice. We also observed that, unlike ND mice, HFD mice failed to mount significant mRNA vaccine-induced $CD8^+$ T cell activation and expression of Th1-associated cytokines including IFNγ, associated with favorable disease outcomes[26, 34]. As IFNγ promotes isotype switching toward IgG2c *in vivo*[35], these two observations are likely linked. Our study is consistent with impaired $CD8^+$ T cell responses following influenza vaccination and natural infection in HFD mice[11, 13, 16]. Furthermore, susceptibility to infection in HFD mice may in part be due to impaired generation of IgG2c Ab subclass, associated with greater effector functions (e.g., induction of phagocytosis, complement fixation) likely important for host defense against infection[36]. Overall, our data demonstrate that HFD obese and diabetic mice have distinct immunity with impaired generation of neutralizing Abs and IFNγ-driven type 1 immunity.

To evaluate whether immunogenicity data translate into protection, we performed a live challenge study. Here, we observed a significant reduction in lung inflammatory responses and lung viral titers relative to PBS-injected mice at day 2 post-infection among ND mice but not in HFD mice. As expected, and in line with immunogenicity data, this result demonstrates that BNT162b2-immunized HFD mice are not protected from challenge, while ND mice are mostly protected. Notably, we did not observe worse disease outcomes (i.e., high viral titers and lung inflammatory responses) in naive, PBS-injected HFD mice compared to ND mice, despite prior observations of more severe disease in HFD animals[19]. However, the shorter duration of follow-

up post challenge, which was chosen to maximize observable differences in lung viral titers, likely accounts for these discrepancies.

By establishing a causal connection between metabolic disease and vaccine efficacy, our study lays the groundwork for future inquiries into the mechanisms behind diminished vaccine responses. T2DM and obesity are characterized by chronic low-grade inflammation, also known as 'metaflammation'[37-41], sharing features with 'inflammaging', the chronic, sterile, low-grade , inflammatory state that characterizes aging[41, 42]. Metaflammation and inflammaging both contribute to the key pathogenesis of metabolomic- or age-related diseases–however, the association and its mechanism on vaccine immunogenicity are not fully elucidated. Senescent cells in older adults provoked CCR2 positive monocyte-dependent inflammation and diminished T cell responses to viruses via secretion of prostaglandin E_2[43]. Interestingly, a short-term inhibition of inflammatory responses boosted adaptive immunity in aged mice[43]. Additionally, T2DM-induced insulin resistance in humans has been linked with impaired ability for $CD14^+$ monocytes to differentiate into dendritic cells (DCs), which then also show reduced classical DC maturation and antigen presenting function[44]. In light of these published studies, our overall findings suggest that hyper-inflammatory states associated with obesity and type 2 DM likely mediated the observed deficits in vaccine response among HFD mice. Future studies should elucidate the mechanistic connections between metabolic disease and vaccine immunogenicity, which could enable implementation of targeted strategies to overcome deficits in vaccine response in vulnerable populations with distinct immunity.

While SARS-CoV-2 vaccines tailored for those with obesity or T2DM do not yet exist, strategies to develop precision vaccines for specific age populations have been investigated. In line with our approach to modeling metabolic disease, age-specific murine models have demonstrated reduced immunogenicity, higher mortality and morbidity, and greater waning immunity in aged mice, comparable to the observations in older adult humans[45-47]. A booster of mRNA vaccine provided sterilizing immunity against Omicron-induced lung infection in aged 21-month-old mice, while younger mice are protected without a booster, indicating the importance of age-specific vaccine regimens[46]. Through the development of an appropriate adjuvant for a SARS-CoV-2 protein-based vaccine, greater protection has been observed in aged mice despite age-related declines in immunity[47]. Based on this precedent, we hypothesize that similar approaches could help overcome metabolic disease-associated deficits in vaccine response. Of note, adjuvants can not only enhance vaccinal immunity but also shape the polarization of the immune response[47, 48]. Defining optimal adjuvant formulation could therefore be a promising approach to overcome the reduced Th1 polarization observed among diabetic obese mice in this study. In combination with further studies elucidating the mechanisms of impaired vaccine responses among those with metabolic disease, an adjuvant approach therefore represents a promising future direction toward effective vaccines tailored to those with T2DM and obesity[49].

Our study has several major strengths, including (a) the comprehensive assessment of a causal connection between metabolic disease and reduced BNT162b2 immunogenicity among neutralizing Abs, IgG2c subclasses, and cytotoxic T cells, and (b) evaluation of protective efficacy from live SARS-CoV-2 challenge. Despite these strengths, we recognize several limitations in the current study, including that (a) only male mice were used due to the increased

425 severity of obesity and insulin resistance in male C57BL/6J mice relative to females[50, 51], (b)
426 only one mouse model was used, establishing the need for future translational research in
427 additional animal models and humans, (c) the overall magnitude of antigen-specific T cell
428 responses were low even after mRNA vaccination due to the use of RBD-specific peptide pool
429 instead of full spike-peptide pool, and (d) although we showed the association with HFD mice
430 and an impairment of type 1 immunity, we were not able to demonstrate the contribution for
431 protection as we had to euthanize mice and collect splenocytes to assess T cell response.
432 Nevertheless, the implications of metabolic disease on BNT162b2 immunogenicity are clear,
433 laying the groundwork for further study into the mechanisms of impaired immune responses,
434 especially focused on a) insulin resistance and b) methods for overcoming these phenomena both
435 in animal models and eventually in the clinic. In parallel to this precision vaccinology approach,
436 public health initiatives that promote physical exercise and a health body weight, both know to
437 help curtail insulin resistance, should be adopted.
438
439 Overall, this study aimed to analyze the effects of obesity and insulin resistance on
440 immunogenicity and protective efficacy following immunization with SARS-CoV-2 BNT162b2
441 mRNA vaccine. We demonstrated that HFD-induced obesity and insulin resistance led to
442 reduced humoral and cellular immunogenicity of the BNT162b2 vaccine. Furthermore, a
443 weakened protective efficacy was shown in HFD mice post BNT162b2 immunization. These
444 observations establish the need to develop precision vaccines against SARS-CoV-2 and other
445 pathogens tailored for those with obesity and DM to overcome impaired immune responses in
446 groups already at high risk of severe infections[52].
447

MATERIALS AND METHODS

Study design. This study aimed to assess the effects of diet-induced obesity and insulin resistance on BNT162b2 mRNA SARS-CoV-2 vaccine immunogenicity and protection in pre-clinical mouse models. To this end, we used longitudinal mouse *in vivo* models fed either a high-fat or control diet to dissect the effects of the high-fat diet and associated phenotypes on vaccine immunogenicity and infection protection. Sample size was chosen empirically based on the results of previous studies and practical limitations such as vivarium capacity. The *in vivo* arm of the study was completed over a single 9-month period, with animal husbandry and associated procedures completed by the same staff throughout. Mouse experiments aimed to include a total of 12–13 mice per group. Mice were randomly assigned to different treatment groups. No data outliers were excluded.

Animals. Male, 14–15-week-old C57BL/6J mice fed on a high-fat or control diet beginning at age 6 weeks were purchased from Jackson Laboratory. Mice were housed under specific pathogen-free conditions at Boston Children's Hospital, and all the procedures were approved under the Institutional Animal Care and Use Committee (IACUC) and operated under the supervision of the Department of Animal Resources at Children's Hospital (ARCH) (Protocol number 00001573). Mice were fed either a high-fat diet containing 60% kcal from fat (D12492i, Research Diets) or an ingredient-matched control diet containing 10% kcal from fat (D12450Ji, Research Diets) from age 6 weeks until the end of the study. At the University of Maryland School of Medicine, mice were housed in a biosafety level 3 (BSL3) facility for all SARS-CoV-2 infections with all the procedures approved under the IACUC (Protocol number #1120004) to MBF.

Fasting Insulin ELISA. Mice were transferred to clean cages without food and fasted for 6 hours. Blood was collected via retro-orbital bleed and serum was isolated by centrifugation at 1500 g for 7.5 minutes. Serum insulin was measured by ELISA according to the manufacturer's wide-range detection protocol (Crystal Chem).

Intraperitoneal glucose tolerance test. An intraperitoneal glucose tolerance test was performed by adapting an existing protocol [22]. Briefly, mice were transferred to clean cages without food, weighed, and fasted for 6 hours. Following fasting, mice were restrained, blood was drawn from the tail vein using a 30-gauge lancet, and baseline blood glucose was measured using a OneTouch Verio Flex meter (LifeScan). A 20% sterile dextrose solution (ICU Medical) was administered via intraperitoneal injection at a final concentration of 2 g dextrose/kg. Blood glucose was measured at 30, 75, and 120 minutes after injection. The resulting values were recorded, and any measurements over the meter's upper limit of detection (600 mg/dL) were assigned a value of 600 mg/dL.

SARS-CoV-2 wildtype spike and RBD expression and purification. Full length SARS-CoV-2 Wuhan-Hu-1 spike glycoprotein (M1-Q1208, GenBank MN90894) and RBD constructs (amino acid residues R319-K529, GenBank MN975262.1), both with an HRV3C protease cleavage site, a TwinStrepTag and an 8XHisTag at C-terminus were obtained from Barney S. Graham (NIH Vaccine Research Center) and Aaron G. Schmidt (Ragon Institute), respectively. These mammalian expression vectors were used to transfect Expi293F suspension cells (Thermo Fisher) using polyethylenimine (Polysciences). Transfected cells were allowed to grow in 37°C,

494 8% CO_2 for an additional 5 days before harvesting for purification. Protein was purified in a PBS
495 buffer (pH 7.4) from filtered supernatants by using either StrepTactin resin (IBA) or Cobalt-
496 TALON resin (Takara). Affinity tags were cleaved off from eluted protein samples by HRV 3C
497 protease, and tag removed proteins were further purified by size-exclusion chromatography using
498 a Superose 6 10/300 column (Cytiva) for full length Spike and a Superdex 75 10/300 Increase
499 column (Cytiva) for RBD domain in a PBS buffer (pH 7.4).
500
501 **Adjuvants and immunization.** BNT162b2 suspension (100 µg/mL) was diluted 1:5 in PBS, and
502 1 µg of mRNA was injected. Mice in the RBD + aluminum hydroxide condition received 10 µg
503 of recombinant monomeric SARS-CoV-2 RBD protein formulated with 100 µg of Alhydrogel
504 adjuvant 2% (Invivogen). Mice in the PBS vaccination group received phosphate-buffered saline
505 (PBS) alone. BNT162b2 spike mRNA vaccine (Pfizer-BioNTech) was obtained as otherwise-to-
506 be-discarded residual volumes in used vials from the Boston Children's Hospital vaccine clinic
507 and was used within 6 hours from the time of reconstitution. Injections (50 µL) were
508 administered intramuscularly in the caudal thigh on days 0 and 14. Blood samples were collected
509 2 weeks post-immunization.
510
511 **Antibody ELISA.** RBD- and spike protein-specific Ab concentrations were quantified in serum
512 samples by ELISA using a previously described protocol [53]. Briefly, high-binding flat-bottom
513 96-well plates (Corning) were coated with 50 ng per well RBD or 25 ng per well spike protein
514 and incubated overnight at 4 °C. Plates were washed with 0.05% Tween 20 PBS and blocked
515 with 1% bovine serum albumin (BSA) in PBS for 1 hour at room temperature. Serum samples
516 were serially diluted 4-fold from 1:100 up to 1:1.05 x 10^8 and then incubated for 2 hours at room

temperature. Plates were washed three times and incubated for 1 hour at room temperature with horseradish peroxidase (HRP)-conjugated anti-mouse IgG, IgG1, IgG2a, or IgG2c (Southern Biotech). Plates were washed five times and developed with tetramethylbenzidine (1-Step Ultra TMB-ELISA Substrate Solution, Thermo Fisher Scientific, for the RBD ELISA, and BD OptEIA Substrate Solution, BD Biosciences, for the spike ELISA) for 5 minutes, then stopped with 2 N H_2SO_4. Optical densities (ODs) were read at 450 nm with a SpectraMax iD3 microplate reader (Molecular Devices). End-point titers were calculated as the dilution that emitted an optical density exceeding a 3× background. An arbitrary value of 50 was assigned to the samples with OD values below the limit of detection for which it was not possible to interpolate the titer.

hACE2-RBD inhibition assay. The hACE2-RBD inhibition assay modified a previously existing protocol [47, 54]. Briefly, high-binding flat-bottom 96-well plates (Corning) were coated with 100 ng per well recombinant human ACE2 (hACE2) (Sigma-Aldrich) in PBS, incubated overnight at 4°C, washed three times with 0.05% Tween 20 PBS, and blocked with 1% BSA PBS for 1 hour at room temperature. Each serum sample was diluted 1:80, pre-incubated with 3 ng of RBD-Fc in 1% BSA PBS for 1 hour at room temperature, and then transferred to the hACE2-coated plate. RBD-Fc without pre-incubation with serum samples was added as a positive control, and 1% BSA PBS without serum pre-incubation was added as a negative control. Plates were then washed three times and incubated with HRP-conjugated anti-human IgG Fc (Southern Biotech) for 1 hour at room temperature. Plates were washed five times and developed with tetramethylbenzidine (BD OptEIA Substrate Solution, BD Biosciences) for 5 min, then stopped with 2 N H_2SO_4. The optical density was read at 450 nm with a SpectraMax iD3 microplate reader (Molecular Devices). Percentage inhibition of RBD binding to hACE2

was calculated with the following formula: Inhibition (%) = [1 – (Sample OD value – Negative Control OD value)/(Positive Control OD value – Negative Control OD value)] x 100.

SARS-CoV-2 neutralization titer determination. All serum samples were heat-inactivated at 56°C for 30 min to deactivate complement and allowed to equilibrate to RT prior to processing for neutralization titer. Samples were diluted in duplicate to an initial dilution of 1:40 followed by 1:2 serial dilutions, resulting in a 12-dilution series with each well containing 60 µl. All dilutions employed DMEM (Quality Biological), supplemented with 10% (v/v) fetal bovine serum (heat-inactivated, Gibco), 1% (v/v) penicillin/streptomycin (Gemini Bio-products) and 1% (v/v) L-glutamine (2 mM final concentration, Gibco). Dilution plates were then transported into the BSL-3 laboratory and 60 µl of diluted SARS-CoV-2 (WA-1, courtesy of Dr. Natalie Thornburg/CDC) inoculum was added to each well to result in a multiplicity of infection (MOI) of 0.01, or 100 pfu/well, upon transfer to titering plates and an initial serum dilution with virus added of 1:80. A non-treated, virus-only control and mock infection control were included on every plate. The sample/virus mixture was then incubated at 37°C (5.0% CO_2) for 1 hour before transferring 100 µl to 96-well titer plates with 1e4 VeroTMPRSS2 cells. Titer plates were incubated at 37°C (5.0% CO_2) for 72 hours, followed by cytopathic effect (CPE) determination for each well in the plate. The first sample dilution to show CPE was reported as the minimum sample dilution required to neutralize >99% of the concentration of SARS-CoV-2 tested (NT_{99}).

Splenocyte restimulation, intracellular cytokine staining and flow cytometry. Mouse spleens were mechanically dissociated and filtered through a 70 µm cell strainer. After centrifugation, cells were treated with 1 mL ammonium-chloride-potassium lysis buffer for 2 minutes at RT. Cells were washed and plated in a 96-well U-bottom plate (2 x 10^6/well) and rested overnight at 37 ºC in RPMI 1640 supplemented with 10% heat-inactivated FBS, penicillin (100 U/ml),

564 streptomycin (100 mg/ml), 2-mercaptoethanol (55 mM), non-essential amino acids (60 mM),
565 HEPES (11 mM), and L-Glutamine (800 mM) (all Gibco). Next day, SARS-CoV-2 RBD peptide
566 pools (PM-WCPV-S-RBD-1, JPT) were added at 0.6 nmol/ml in the presence of anti-mouse
567 CD28/49d (1 µg/mL, BD) and brefeldin A (5 µg/ml, BioLegend). After a 6-hour stimulation,
568 cells were washed twice and treated with Mouse Fc Block (BD) according to the manufacturer's
569 instructions. Cells were washed and stained with Aqua Live/Dead stain (Life Technologies,
570 1:500) for 15 minutes at RT. Following two additional washes, cells were incubated with the
571 following Abs for 30 minutes at 4°C: anti-mouse CD44 [IM7, PerCP-Cy5.5, BioLegend
572 #103032, 1:160], anti-mouse CD3 [17A2, Brilliant Violet 785, BioLegend #100232, 1:40], anti-
573 mouse CD4 [RM4-5, APC/Fire 750, BioLegend 100568, 1:160] and anti-mouse CD8 [53-6.7,
574 Brilliant UltraViolet 395, BD #563786, 1:80]. Cells were then fixed and permeabilized by using
575 the BD Cytofix/Cytoperm kit according to the manufacturer's instructions and were subjected to
576 intracellular staining (30 minutes at 4 °C) using the following Abs: anti-mouse IFNγ [XMG1.2,
577 Alexa Fluor 488, BioLegend #505813, 1:160], anti-mouse TNF [MP6-XT22, PE Cy7,
578 BioLegend # 506324, 1:160], anti-mouse IL-2 [JES6-5H4, PE, BioLegend # 503808, 1:40].
579 Finally, cells were fixed in 1% paraformaldehyde (Electron Microscopy Sciences) for 20 minutes
580 at 4 ºC and stored in PBS at 4 ºC until acquisition. Samples were analyzed on an LSR Fortessa
581 (BD) flow cytometer and FlowJo v10.8.1 (FlowJo LLC).
582
583 **SARS-CoV-2 mouse challenge study.** Mice were anesthetized by intraperitoneal injection of 50
584 µL of a mix of xylazine (0.38 mg/mouse) and ketamine (1.3 mg/mouse) diluted in PBS. Mice
585 were then intranasally inoculated with 1 x 10^3 PFU of mouse-adapted SARS-CoV-2 (MA10,
586 courtesy of Dr. Ralph Baric (UNC)) in 50 µL divided between nares [27]. Challenged mice were

weighed on the day of infection and daily for up to 2 days post-infection. At 2 days post-infection, mice were euthanized, and lungs were harvested to determine virus titer by a plaque assay and prepared for histological staining and RNA extraction.

SARS-CoV-2 plaque assay. The day prior to infection, 2.5e5 VeroTMPRSS2 cells were seeded per well in a 12-well plate in 1mL of VeroTMPRSS2 media. Tissue samples were thawed and homogenized with 1mm beads in an Omni Bead ruptor (Omni International Inc., Kennesaw, GA) and then spun down at 21,000 g for 2 minutes. A 6-point dilution curve was prepared by serial diluting 25 µL of sample 1:10 in 225 µL DMEM. 200 µL of each dilution was then added to the cells and the plates were rocked every 15 minutes for 1 hour at 37°C. After 1 hr, 2 mL of a semi-solid agarose overlay was added to each well (DMEM, 4% FBS, 0.06% UltraPure agarose (Invitrogen, Carlsbad, CA). After 48 hours at 37°C and 5% CO_2, plates were fixed in 2% PFA for 20 minutes, stained with 0.5 mL of 0.05% Crystal Violet and 20% EtOH, and washed 2x with H_2O prior to counting of plaques. The titer was then calculated. For tissue homogenates, this titer was multiplied by 40 based on the average tissue sample weight being 25 mg.

Gene expression analysis by qPCR. RNA was isolated from TRI Reagent samples using phenol-chloroform extraction or column-based extraction systems (Direct-zol RNA Miniprep, Zymo Research) according to the manufacturer's protocol. RNA concentration and purity (260/280 and 260/230 ratios) were measured by NanoDrop (Thermo Fisher Scientific). Samples with an A260/A280 ratio of <1.8 were excluded for further analysis. cDNA was prepared from purified RNA with RT2 First Strand Kit, per the manufacturer's instructions (Qiagen). cDNA was quantified by qPCR on a 7300 real-time PCR system (Applied Biosystems) using pre-

designed SYBR Green Primers (QIAGEN) specific for *Ifit2* (PPM05993A), *Cxcl10* (PPM02978A), *Csf2* (PPM02990A), *Il6* (PPM03015A), *Ccl2* (PPM03151A), *Cxcl1* (PPM03058A), and *Actb* (PPM02945A).

Histopathology analysis. Slides were prepared as 5 μm sections and stained with hematoxylin and eosin. A pathologist was blinded to information identifying the treatment groups and fields were examined by light microscopy.

Statistical analysis. Statistical analyses employed Prism v9.4.0 (GraphPad Software). *P* values < 0.05 were considered significant. Normally distributed data were analyzed by t-test or one- or two-way analyses of variance (ANOVAs). To achieve normal distribution, some datasets were analyzed after Log-transformation as indicated in the figure legends. Non-normally distributed data were analyzed by Mann-Whitney U-test or Kruskal-Wallis test. *P* values were corrected for multiple comparisons.

LIST OF SUPPLEMENTARY MATERIALS

Figures S1 to S3

Table S1

REFERENCES

1. S. Bryan JA, M. Carroll, C. Te-Ching, D. Orlando, S. Fink, C. Fryar, NHSR 158. National Health and Nutrition Examination Survey 2017–March 2020 Pre-pandemic Data Files (National Center for Health Statistics (U.S.), 2021; http://dx.doi.org/10.15620/cdc:106273).
2. Pearson-Stuttard J, Blundell S, Harris T, Cook DG, Critchley J. Diabetes and infection: assessing the association with glycaemic control in population-based studies. Lancet Diabetes Endocrinol 2016; 4:148-58.
3. Antos A, Kwong ML, Balmorez T, Villanueva A, Murakami S. Unusually High Risks of COVID-19 Mortality with Age-Related Comorbidities: An Adjusted Meta-Analysis Method to Improve the Risk Assessment of Mortality Using the Comorbid Mortality Data. Infect Dis Rep 2021; 13:700-11.
4. Williamson EJ, Walker AJ, Bhaskaran K, Bacon S, Bates C, Morton CE, et al. Factors associated with COVID-19-related death using OpenSAFELY. Nature 2020; 584:430-6.
5. Holman N, Knighton P, Kar P, O'Keefe J, Curley M, Weaver A, et al. Risk factors for COVID-19-related mortality in people with type 1 and type 2 diabetes in England: a population-based cohort study. Lancet Diabetes Endocrinol 2020; 8:823-33.
6. Lim S, Bae JH, Kwon HS, Nauck MA. COVID-19 and diabetes mellitus: from pathophysiology to clinical management. Nat Rev Endocrinol 2021; 17:11-30.
7. Marfella R, Sardu C, D'Onofrio N, Prattichizzo F, Scisciola L, Messina V, et al. Glycaemic control is associated with SARS-CoV-2 breakthrough infections in vaccinated patients with type 2 diabetes. Nat Commun 2022; 13:2318.

8. Soetedjo NNM, Iryaningrum MR, Lawrensia S, Permana H. Antibody response following SARS-CoV-2 vaccination among patients with type 2 diabetes mellitus: A systematic review. Diabetes Metab Syndr 2022; 16:102406.

9. Yamamoto S, Mizoue T, Tanaka A, Oshiro Y, Inamura N, Konishi M, et al. Sex-associated differences between BMI and SARS-CoV-2 antibody titers following the BNT162b2 vaccine. Obesity (Silver Spring) 2022; 30:999-1003.

10. Milner JJ, Rebeles J, Dhungana S, Stewart DA, Sumner SC, Meyers MH, et al. Obesity Increases Mortality and Modulates the Lung Metabolome during Pandemic H1N1 Influenza Virus Infection in Mice. J Immunol 2015; 194:4846-59.

11. Karlsson EA, Sheridan PA, Beck MA. Diet-induced obesity in mice reduces the maintenance of influenza-specific CD8+ memory T cells. J Nutr 2010; 140:1691-7.

12. Milner JJ, Sheridan PA, Karlsson EA, Schultz-Cherry S, Shi Q, Beck MA. Diet-induced obese mice exhibit altered heterologous immunity during a secondary 2009 pandemic H1N1 infection. J Immunol 2013; 191:2474-85.

13. Karlsson EA, Sheridan PA, Beck MA. Diet-induced obesity impairs the T cell memory response to influenza virus infection. J Immunol 2010; 184:3127-33.

14. Kosaraju R, Guesdon W, Crouch MJ, Teague HL, Sullivan EM, Karlsson EA, et al. B Cell Activity Is Impaired in Human and Mouse Obesity and Is Responsive to an Essential Fatty Acid upon Murine Influenza Infection. J Immunol 2017; 198:4738-52.

15. Kim YH, Kim JK, Kim DJ, Nam JH, Shim SM, Choi YK, et al. Diet-induced obesity dramatically reduces the efficacy of a 2009 pandemic H1N1 vaccine in a mouse model. J Infect Dis 2012; 205:244-51.

673 16. Park HL, Shim SH, Lee EY, Cho W, Park S, Jeon HJ, et al. Obesity-induced chronic
674 inflammation is associated with the reduced efficacy of influenza vaccine. Hum Vaccin
675 Immunother 2014; 10:1181-6.
676 17. Karlsson EA, Hertz T, Johnson C, Mehle A, Krammer F, Schultz-Cherry S. Obesity
677 Outweighs Protection Conferred by Adjuvanted Influenza Vaccination. mBio 2016; 7.
678 18. Cho WJ, Lee DK, Lee SY, Sohn SH, Park HL, Park YW, et al. Diet-induced obesity
679 reduces the production of influenza vaccine-induced antibodies via impaired macrophage
680 function. Acta Virol 2016; 60:298-306.
681 19. Rathnasinghe R, Jangra S, Cupic A, Martinez-Romero C, Mulder LCF, Kehrer T, et al.
682 The N501Y mutation in SARS-CoV-2 spike leads to morbidity in obese and aged mice
683 and is neutralized by convalescent and post-vaccination human sera. medRxiv 2021.
684 20. Lee KS, Russ BP, Wong TY, Horspool AM, Winters MT, Barbier M, et al. Diet induced
685 obesity and type 2 diabetes drives exacerbated sex-associated disease profiles in K18-
686 hACE2-mice challenged with SARS-CoV-2. bioRxiv 2022:2022.04.26.489580.
687 21. Kulcsar KA, Coleman CM, Beck SE, Frieman MB. Comorbid diabetes results in immune
688 dysregulation and enhanced disease severity following MERS-CoV infection. JCI Insight
689 2019; 4.
690 22. Andrikopoulos S, Blair AR, Deluca N, Fam BC, Proietto J. Evaluating the glucose
691 tolerance test in mice. Am J Physiol Endocrinol Metab 2008; 295:E1323-32.
692 23. Heydemann A. An Overview of Murine High Fat Diet as a Model for Type 2 Diabetes
693 Mellitus. J Diabetes Res 2016; 2016:2902351.

24. Li C, Lee A, Grigoryan L, Arunachalam PS, Scott MKD, Trisal M, et al. Mechanisms of innate and adaptive immunity to the Pfizer-BioNTech BNT162b2 vaccine. Nat Immunol 2022; 23:543-55.

25. Laczko D, Hogan MJ, Toulmin SA, Hicks P, Lederer K, Gaudette BT, et al. A Single Immunization with Nucleoside-Modified mRNA Vaccines Elicits Strong Cellular and Humoral Immune Responses against SARS-CoV-2 in Mice. Immunity 2020; 53:724-32 e7.

26. Liu J, Yu J, McMahan K, Jacob-Dolan C, He X, Giffin V, et al. CD8 T Cells Contribute to Vaccine Protection Against SARS-CoV-2 in Macaques. Sci Immunol 2022:eabq7647.

27. Leist SR, Dinnon KH, 3rd, Schafer A, Tse LV, Okuda K, Hou YJ, et al. A Mouse-Adapted SARS-CoV-2 Induces Acute Lung Injury and Mortality in Standard Laboratory Mice. Cell 2020; 183:1070-85 e12.

28. Israelow B, Song E, Mao T, Lu P, Meir A, Liu F, et al. Mouse model of SARS-CoV-2 reveals inflammatory role of type I interferon signaling. J Exp Med 2020; 217.

29. Coperchini F, Chiovato L, Croce L, Magri F, Rotondi M. The cytokine storm in COVID-19: An overview of the involvement of the chemokine/chemokine-receptor system. Cytokine Growth Factor Rev 2020; 53:25-32.

30. Del Valle DM, Kim-Schulze S, Huang HH, Beckmann ND, Nirenberg S, Wang B, et al. An inflammatory cytokine signature predicts COVID-19 severity and survival. Nat Med 2020; 26:1636-43.

31. Zaid Y, Doré É, Dubuc I, Archambault AS, Flamand O, Laviolette M, et al. Chemokines and eicosanoids fuel the hyperinflammation within the lungs of patients with severe COVID-19. J Allergy Clin Immunol 2021; 148:368-80.e3.

717 32. Thwaites RS, Sanchez Sevilla Uruchurtu A, Siggins MK, Liew F, Russell CD, Moore SC,
718 et al. Inflammatory profiles across the spectrum of disease reveal a distinct role for GM-
719 CSF in severe COVID-19. Sci Immunol 2021; 6.
720 33. People with Certain Medical Conditions. 2022.] Available from
721 https://www.cdc.gov/coronavirus/2019-ncov/need-extra-precautions/people-with-
722 medical-conditions.html.
723 34. Gil-Etayo FJ, Garcinuno S, Utrero-Rico A, Cabrera-Marante O, Arroyo-Sanchez D,
724 Mancebo E, et al. An Early Th1 Response Is a Key Factor for a Favorable COVID-19
725 Evolution. Biomedicines 2022; 10.
726 35. Miyauchi K, Sugimoto-Ishige A, Harada Y, Adachi Y, Usami Y, Kaji T, et al. Protective
727 neutralizing influenza antibody response in the absence of T follicular helper cells. Nat
728 Immunol 2016; 17:1447-58.
729 36. Bournazos S, Ravetch JV. Fcγ Receptor Function and the Design of Vaccination
730 Strategies. Immunity 2017; 47:224-33.
731 37. Berbudi A, Rahmadika N, Tjahjadi AI, Ruslami R. Type 2 Diabetes and its Impact on the
732 Immune System. Curr Diabetes Rev 2020; 16:442-9.
733 38. Ferlita S, Yegiazaryan A, Noori N, Lal G, Nguyen T, To K, et al. Type 2 Diabetes
734 Mellitus and Altered Immune System Leading to Susceptibility to Pathogens, Especially
735 Mycobacterium tuberculosis. J Clin Med 2019; 8.
736 39. de Heredia FP, Gomez-Martinez S, Marcos A. Obesity, inflammation and the immune
737 system. Proc Nutr Soc 2012; 71:332-8.
738 40. Marti A, Marcos A, Martinez JA. Obesity and immune function relationships. Obes Rev
739 2001; 2:131-40.

740 41. Prattichizzo F, De Nigris V, Spiga R, Mancuso E, La Sala L, Antonicelli R, et al.
741 Inflammageing and metaflammation: The yin and yang of type 2 diabetes. Ageing Res
742 Rev 2018; 41:1-17.
743 42. Franceschi C, Garagnani P, Parini P, Giuliani C, Santoro A. Inflammaging: a new
744 immune-metabolic viewpoint for age-related diseases. Nat Rev Endocrinol 2018; 14:576-
745 90.
746 43. Chambers ES, Vukmanovic-Stejic M, Shih BB, Trahair H, Subramanian P, Devine OP, et
747 al. Recruitment of inflammatory monocytes by senescent fibroblasts inhibits antigen-
748 specific tissue immunity during human aging. Nature Aging 2021; 1:101-13.
749 44. Paccosi S, Pala L, Cresci B, Silvano A, Cecchi M, Caporale R, et al. Insulin resistance
750 and obesity affect monocyte-derived dendritic cell phenotype and function. Diabetes Res
751 Clin Pract 2020; 170:108528.
752 45. Collier DA, Ferreira I, Kotagiri P, Datir RP, Lim EY, Touizer E, et al. Age-related
753 immune response heterogeneity to SARS-CoV-2 vaccine BNT162b2. Nature 2021;
754 596:417-22.
755 46. Nanishi E, McGrath ME, O'Meara TR, Barman S, Yu J, Wan H, et al. mRNA booster
756 vaccination protects aged mice against the SARS-CoV-2 Omicron variant. Commun Biol
757 2022; 5:790.
758 47. Nanishi E, Borriello F, O'Meara TR, McGrath ME, Saito Y, Haupt RE, et al. An
759 aluminum hydroxide:CpG adjuvant enhances protection elicited by a SARS-CoV-2
760 receptor binding domain vaccine in aged mice. Sci Transl Med 2022; 14:eabj5305.
761 48. Nanishi E, Dowling DJ, Levy O. Toward precision adjuvants: optimizing science and
762 safety. Curr Opin Pediatr 2020; 32:125-38.

763 49. Schijns V, Fernández-Tejada A, Barjaktarović Ž, Bouzalas I, Brimnes J, Chernysh S, et
764 al. Modulation of immune responses using adjuvants to facilitate therapeutic vaccination.
765 Immunol Rev 2020; 296:169-90.
766 50. Maric I, Krieger JP, van der Velden P, Börchers S, Asker M, Vujicic M, et al. Sex and
767 Species Differences in the Development of Diet-Induced Obesity and Metabolic
768 Disturbances in Rodents. Front Nutr 2022; 9:828522.
769 51. Pettersson US, Waldén TB, Carlsson PO, Jansson L, Phillipson M. Female mice are
770 protected against high-fat diet induced metabolic syndrome and increase the regulatory T
771 cell population in adipose tissue. PLoS One 2012; 7:e46057.
772 52. Dowling DJ, Levy O. A Precision Adjuvant Approach to Enhance Severe Acute
773 Respiratory Syndrome Coronavirus 2 (SARS-CoV-2) Vaccines Optimized for
774 Immunologically Distinct Vulnerable Populations. Clin Infect Dis 2022; 75:S30-s6.
775 53. Borriello F, Pietrasanta C, Lai JCY, Walsh LM, Sharma P, O'Driscoll DN, et al.
776 Identification and Characterization of Stimulator of Interferon Genes As a Robust
777 Adjuvant Target for Early Life Immunization. Front Immunol 2017; 8:1772.
778 54. Tan CW, Chia WN, Qin X, Liu P, Chen MI, Tiu C, et al. A SARS-CoV-2 surrogate virus
779 neutralization test based on antibody-mediated blockage of ACE2-spike protein-protein
780 interaction. Nat Biotechnol 2020; 38:1073-8.
781

ACKNOWLEDGEMENTS

We thank the members of the BCH *Precision Vaccines Program* (PVP) for helpful discussions as well as Kevin Churchwell, Gary Fleisher, David Williams, and August Cervini for their support of the PVP. We thank Ralph Baric for providing the SARS-CoV-2/MA10 virus. We thank B. S. Graham (NIH Vaccine Research Center) for providing the plasmid for prefusion stabilized SARS-CoV-2 spike trimer and Aaron G. Schmidt for providing the spike RBD constructs used for protein expression. We thank the pharmacists of BCH for their efforts to maximize the use of SARS-CoV-2 vaccines by saving leftover or to-be-discarded overfill from BNT162b2 vaccine vials. E.N. is a JSPS Overseas Research Fellow and a joint Society for Pediatric Research and Japanese Pediatric Society Scholar. D.J.D. thanks Siobhan McHugh, Geneva Boyer, Lucy Conetta, and the staff of Lucy's Daycare, the staff of YMCA of Greater Boston, Bridging Independent Living Together (BILT), Inc., and the Boston Public Schools for childcare and educational support during the COVID-19 pandemic. The graphics in **Fig.1A** and **2A** were created with BioRender.

Category	Ingredient	D12492i High-Fat Diet % by Weight	D12450Ji Control Diet % by Weight
Protein	Casein, Lactic, 30 Mesh	25.84	18.96
Protein	L Cystine	0.39	0.28
Carbohydrate	Lodex 10 (Maltodextrin)	16.15	11.85
Carbohydrate	Fine Granulated Sucrose	9.41	6.90
Carbohydrate	Starch, Corn	0	47.98
Fiber	Solka Floc, FCC200	6.46	4.74
Fat	Lard	31.66	1.90
Fat	Soybean Oil, USP	3.23	2.37
Mineral	S10026B Mineral Mix (Research Diets)	6.46	4.74
Vitamin	Choline Bitartrate	0.26	0.19
Vitamin	V10001C Vitamin Mix (Research Diets)	0.13	0.09
Dye	Blue FD&C #1, Alum. Lake 35-42%	0.0065	0.0009
Dye	Yellow FD&C #5, Alum. Lake 35-42%	0	0.0038

Supplementary Table 1. Composition of high-fat and control diets.
High-fat diet D12492i (Research Diets) comprised of 60% kcal from fat and control diet D12450Ji (Research Diets) comprised of 10% kcal from fat were fed to male C57BL/6J mice.

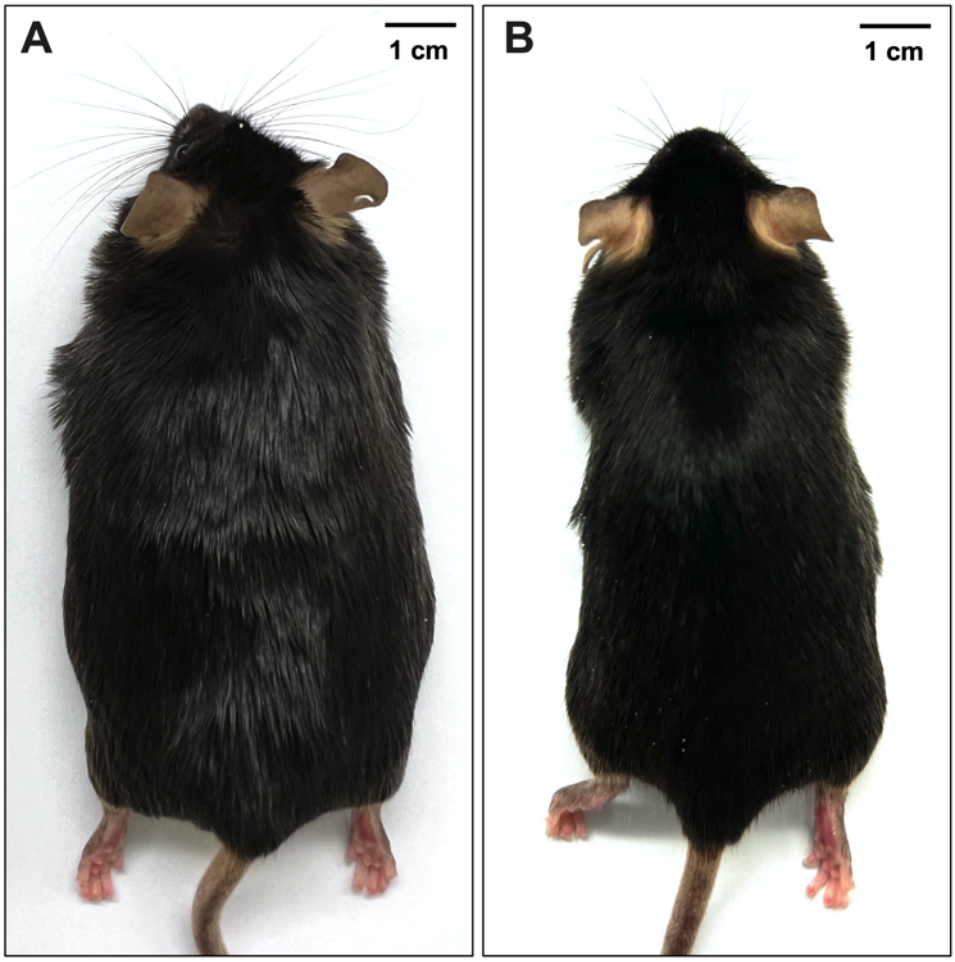

Supplementary Figure 1. A high-fat diet induces obesity in male C57BL/6J mice.
Representative images of (A) diet-induced obese and (B) control male C57BL/6J mice at age 30 weeks.

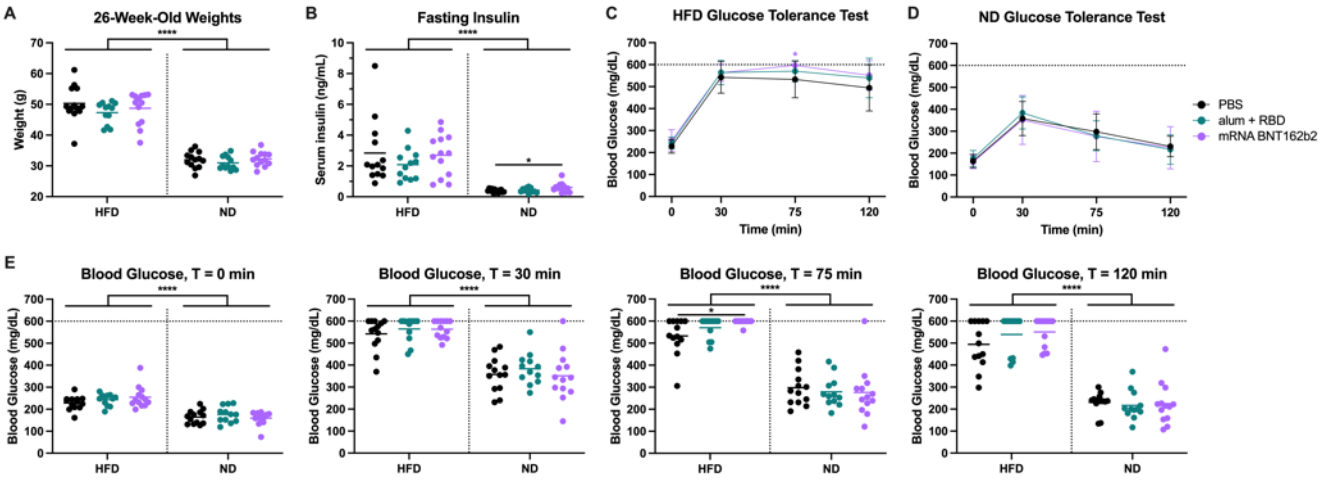

Supplementary Figure 2. Obesity, hyperglycemia, and poor glucose tolerance phenotypes are comparable across vaccine treatment groups within each strain.

(A) Mice were weighed during the week of the first immunization. Weights are grouped by vaccine condition and mouse diet (HDF or ND). (B) Serum insulin levels were measured after a 6-hour fast. (C–E) Glucose tolerance was assessed by measuring blood glucose at time points 0, 30, 75, and 120 min following a 6-hour fast and intraperitoneal injection of 2 g/kg dextrose. Blood glucose values above the glucometer's 600 mg/dL upper limit of detection were assigned a value of 600 mg/dL. Longitudinal graphs display mean and SD of HFD (C) and ND (D) strains. Bars represent means in all dotplots. Horizontal dotted lines represent upper limits of detection. n = 13 per group in the PBS and mRNA BNT 162b2 groups and n = 12 in the alum + RBD group across both strains. Significance within each strain was assessed by Kruskal-Wallis test with post-hoc Dunn's multiple comparisons test. Comparisons between HFD and ND mice were assessed by unpaired t-test (A, B) or Mann-Whitney U tests (E). * $P < 0.05$ and **** $P < 0.0001$.

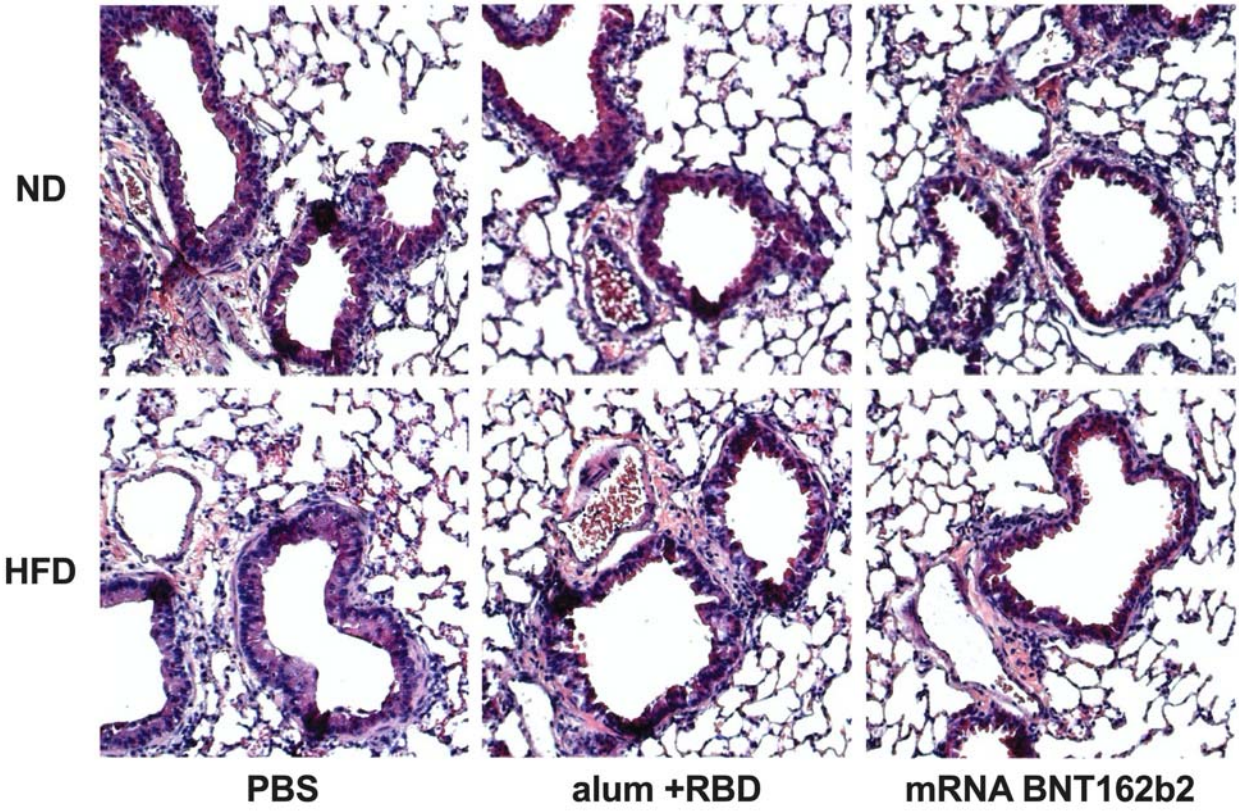

Supplementary Figure 3. Lung histopathology following live SARS-CoV-2 MA10 challenge. Lung tissue was harvested at 2 days post challenge, fixed, sectioned, and stained using hematoxylin and eosin. Representative images are shown. N = 6–7 per group.